Effect of Ancillary Ligands on Ru(II) on Electronic Delocalization in Ruthenium(II) Bisferrocenylacetylide Complexes

Yongbao Zhu, Olivier Clot, Michael O. Wolf,* and Glenn P. A. Yap[†]

Contribution from the Department of Chemistry, The University of British Columbia, Vancouver British Columbia, Canada V6T 1Z1, and Department of Chemistry and Biochemistry, University of Windsor, Windsor, Canada N9B 3P4

Received September 15, 1997

Abstract: The synthesis and properties of [*cis*-Ru(dppm)$_2$(C≡CFc)$_2$]CuI (dppm = $Ph_2PCH_2PPh_2$, Fc = ferrocenyl) (**1**) and *trans*,*trans*,*trans*-Ru(PBu_3)$_2$(CO)(L)(C≡CFc)$_2$ (**3**, L = CO; **4**, L = pyridine; **5**, L = $P(OMe)_3$) are reported. The ruthenium bisacetylide bridges in these complexes allow electronic interaction between the terminal ferrocenyl groups. The interaction is enhanced when the ancillary ligands on the ruthenium center are electron donors and lessened when the ligands are acceptors. Complex **1** was prepared in 70% yield by the coupling of FcC≡CSn(*n*-Bu)$_3$ and cis- or *trans*-$RuCl_2$(dppm)$_2$ in the presence of excess CuI and was crystallographically characterized. Removal of the coordinated CuI from **1** with excess $P(OMe)_3$ yields *trans*-Ru(dppm)$_2$(C≡CFc)$_2$ (**2**). Reaction of **2** with CuI yields **1**. *trans*,*trans*,*trans*-Ru(PBu_3)$_2$(CO)$_2$(C≡CFc)$_2$ (**3**) was synthesized from $RuCl_2(CO)_2(PBu_3)_2$ and FcC≡CSn(*n*-Bu)$_3$ using a CuI catalyst and was crystallographically characterized. Reaction of **3** with excess pyridine yields *trans*,*trans*,*trans*-Ru(PBu_3)$_2$(CO)(py)(C≡CFc)$_2$ (**4**). The reaction is reversible; **3** may be obtained by reacting **4** with excess carbon monoxide. Reaction of **4** with $P(OMe)_3$ yields *trans*,*trans*,*trans*-Ru(PBu_3)$_2$(CO)($P(OMe)_3$)(C≡CFc)$_2$ (**5**). Dications of all the complexes were prepared by oxidation with 2 equiv of $FcPF_6$, and monocations were prepared in solution by reaction of the neutral complexes with the dications. The difference between the first and second ferrocenyl oxidations ($\Delta E_{1/2}$) in the cyclic voltammograms of **1**, **3**, **4**, and **5** are 0.14, 0.09, 0.13, and 0.15 V, respectively. Characterization of the complexes by visible, IR, and near-IR spectroscopy supports the conclusion that the ligand environment of the ruthenium center affects the extent of electronic delocalization between the ferrocenyl groups.

Introduction

Polymers and oligomers containing metal groups linked by conjugated moieties are of interest because of the possibility of metal-enhanced charge transfer along the backbone involving the metal group. A number of metal-containing conjugated polymers are known,[1−25] but these materials are generally poorly conducting or insulating.[3,12] A significant challenge in this field is to determine why such polymers are not good conductors in comparison to the purely organic analogues, and ultimately to prepare new materials which are better conductors.

Metal-containing conjugated polymers will only be conducting if charge carriers can be delocalized over both the metal and organic fragments. There are many known conjugated organic polymers which delocalize charge very well when doped;[2] we have therefore focused our efforts on finding a suitable metal bridging group. Metal bisacetylide bridges are good candidates because they are stable under the oxidizing conditions which are typically used to dope conducting polymers and to inject charge carriers. They are also synthetically accessible for a large number of different metal ligand combinations.[26] Electron delocalization over a metal bisacetylide bridge can be probed by examining the behavior of molecules in which

[†] Current address: University of Ottawa X-ray Laboratory, Ottawa ON, K1N 6N5 Canada.

(1) McDermott, J. X.; White, J. F.; Whitesides, G. M. *J. Am. Chem. Soc.* **1976**, *98*, 6521−6528.
(2) Skotheim, T. A. *Handbook of Conducting Polymers*; Marcel Dekker: New York, 1986.
(3) Hagihara, N.; Sonogashira, K.; Takahashi, S. *Adv. Polym. Sci.* **1981**, *41*, 149−179.
(4) Marder, T. B.; Lesley, G.; Yuan, Z.; Fyfe, H. B.; Chow, P.; Stringer, G.; Jobe, I. R.; Taylor, N. J.; Williams, I. D.; Kurtz, S. K. *ACS Symp. Ser.* **1991**, *455*, 606−615.
(5) Kittlesen, G. P.; White, H. S.; Wrighton, M. S. *J. Am. Chem. Soc.* **1984**, *106*, 7389−7396.
(6) Hush, N. S. *Prog. Inorg. Chem.* **1967**, *8*, 391−444.
(7) Sonogashira, K.; Kataoka, S.; Takahashi, S.; Hagihara, N. *J. Organomet. Chem.* **1978**, *160*, 319−327.
(8) Stang, P. J.; Tykwinski, R. *J. Am. Chem. Soc.* **1992**, *114*, 4411−4412.
(9) Sonogashira, K.; Ohga, K.; Takahashi, S.; Hagihara, N. *J. Organomet. Chem.* **1980**, *188*, 237−243.
(10) Sullivan, B. P.; Meyer, T. J. *Inorg. Chem.* **1982**, *21*, 1027−1040.
(11) Sun, Y.; Taylor, N. J.; Carty, A. J. *Organometallics* **1992**, *11*, 4293−4300.
(12) Nast, R.; Grouhi, H. *J. Organomet. Chem.* **1979**, *182*, 197−202.
(13) Jenekhe, S. A. *Macromolecules* **1990**, *23*, 2848−2854.
(14) Field, L. D.; George, A. V.; Hambley, T. W.; Malouf, E. Y.; Young, D. J. *J. Chem. Soc., Chem. Commun.* **1990**, 931−933.
(15) Ochmanska, J.; Pickup, P. G. *Can. J. Chem.* **1991**, *69*, 653−660.
(16) Ofer, D.; Wrighton, M. S. *J. Am. Chem. Soc.* **1988**, *110*, 4467−4468.
(17) Fujikura, Y.; Sonogashira, K.; Hagihara, N. *Chem. Lett.* **1975**, 1067−1070.
(18) Fyfe, H. B.; Mlekuz, M.; Zargarian, D.; Taylor, N. J.; Marder, T. B. *J. Chem. Soc., Chem. Commun.* **1991**, 188−190.
(19) Ingham, S. L.; Khan, M. S.; Lewis, J.; Long, N. J.; Raithby, P. R. *J. Organomet. Chem.* **1994**, *470*, 153−159.
(20) Nalwa, H. S. *Appl. Organomet. Chem.* **1990**, *4*, 91−102.
(21) Natan, M. J.; Wrighton, M. S. In *Progress in Inorganic Chemistry*; Lippard, S. J., Ed.; John Wiley and Sons: New York, 1989; Vol. 37.
(22) Park, L. Y.; Ofer, D.; Gardner, T. J.; Schrock, R. R.; Wrighton, M. S. *Chem. Mater.* **1992**, *4*, 1388−1395.
(23) Takahashi, S.; Ohyama, Y.; Murata, E.; Sonogashira, K.; Hagihara, N. *J. Polym. Sci. Polym. Chem. Educ.* **1980**, *18*, 349−353.
(24) Takahashi, S.; Morimoto, H.; Murata, E.; Kataoka, S.; Sonogashira, K.; Hagihara, N. *J. Polym. Sci. Polym. Chem. Educ.* **1982**, *20*, 565−573.
(25) Wright, M. E. *Macromolecules* **1989**, *22*, 3256−3259.

S0002-7863(97)03248-4 CCC: $15.00
Published on Web 02/10/1998

Scheme 1

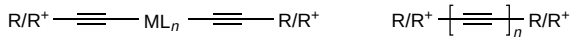

(a) (b)

the bridge of interest spans two redox groups (Scheme 1a). We and others have recently demonstrated that platinum[27] and ruthenium[28,29] bisacetylide complexes show electronic interaction between terminal redox groups, suggesting that these moieties are capable of delocalizing charge. Additionally, oligoacetylide chains terminated with redox-active organometallic terminal groups often show significant interaction between the terminal groups.[8,30−32] These systems allow one to probe electron transfer along extended acetylide ligands (Scheme 1b).

In this paper, we report the effect of the ancillary ligands (L) of $RuL_4(C{\equiv}CFc)_2$ (Fc = ferrocenyl) complexes on the electronic interaction between the terminal redox groups. We explore the effect of isomerization by examining [*cis*-Ru(dppm)$_2$(C≡CFc)$_2$]-CuI (dppm = $Ph_2PCH_2PPh_2$) (**1**) and comparing its electronic properties with those of the previously reported *trans*-Ru-(dppm)$_2$(C≡CFc)$_2$ (**2**).[29] The effect of the ligand environment at the ruthenium in a series of trans substituted complexes is investigated by the electrochemical and spectroscopic characterization of $Ru(PBu_3)_2(CO)(L)(C{\equiv}CFc)_2$ complexes (L = CO (**3**); L = pyridyl (**4**); L = $P(OMe)_3$ (**5**)) and their mono- and dications.

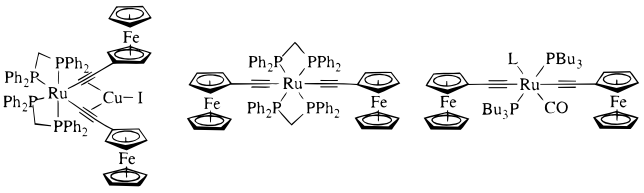

1 **2** **3** L = CO; **4** L = C_5H_5N; **5** L = $P(OMe)_3$

Experimental Section

General. *trans*-$RuCl_2(dppm)_2$,[33] *cis*-$RuCl_2(dppm)_2$,[10] $FcPF_6$,[34] and FcC≡CSn(*n*-Bu)$_3$[29] were all prepared by using literature procedures. *trans*-$RuCl_2(PBu_3)_2(CO)_2$ was prepared by using the literature procedure for the preparation of *trans*-$RuCl_2(PEt_3)_2(CO)_2$.[33] All other reagents were purchased from either Strem Chemicals or Aldrich and used as received. Electronic absorption spectra were obtained on a UNICAM UV2 UV−vis spectrometer. Near-IR data were obtained on a Varian Cary 5 spectrometer. Extinction coefficients and absorption maxima for overlapping near-IR bands were determined by fitting the data to multiple Gaussians. IR data were collected on a UNICAM Galaxy Series FTIR 5000 spectrometer. ^{1}H and ^{31}P{^{1}H} NMR experiments were performed on either a Bruker CPX-200, Varian XL-300, or Bruker WH-400 spectrometer. Spectra were referenced to residual solvent (^{1}H) or external 85% H_3PO_4 (^{31}P). Electrochemical measurements were conducted on a Pine AFCBP1 bipotentiostat using a Pt disk working electrode, Pt coil wire counter electrode, and saturated calomel reference electrode (SCE). The supporting electrolyte was 0.1 M [(*n*-Bu)$_4$N]-PF_6, which was purified by triple recrystallization from ethanol and dried at 90 °C under vacuum for 3 days. Methylene chloride used in cyclic voltammetry was dried by refluxing over CaH_2.

[*cis*-Ru(dppm)$_2$(C≡CFc)$_2$]CuI (1). To a solution of FcC≡CSn-(*n*-Bu)$_3$ (1.10 g, 2.20 mmol) in CH_2Cl_2 (70 mL) under a nitrogen atmosphere was added *cis*-$RuCl_2(dppm)_2$ (0.82 g, 0.87 mmol) and CuI (0.26 g, 1.4 mmol). The red-brown suspension was stirred at 25 °C for 72 h. The cloudy solution was filtered through Celite 545 and the volume of the solution reduced to approximately 4 mL and hexanes (100 mL) were added to precipitate a yellow-brown solid. The solid was dissolved in CH_2Cl_2 (50 mL) and a solution of sodium iodide (2.1 g, 14 mmol) in acetone (30 mL) added. The solution turned cloudy after stirring at room temperature for 2 h, whereupon the solvent was removed and chloroform (20 mL) added. The undissolved solids were removed by filtration, and the filtrate was concentrated and hexanes added until the solution was almost saturated. A yellow-orange crystalline solid precipitated after the solution was cooled to −10 °C. The solid was dissolved in a small amount of choroform and reprecipitated by adding hexanes. The resulting powder was dried under vacuum at room temperature for 3 days. Yield: 0.94 g (72%). ^{1}H NMR (400 MHz, CD_2Cl_2): δ 8.23 (m, 4 H, phenyl), 8.03 (m, 4 H, phenyl), 7.50−7.15 (m, 24 H, phenyl), 6.86 (t, J_{HH} = 7.1 Hz, 4 H, phenyl), 6.39 (t, J_{HH} = 8.2 Hz, 4 H, phenyl), 4.67 (m, 2H, C_5H_4), 4.72−4.62 (m, 2 H, CH_2), 4.40−4.30 (m, 2H, CH_2), 4.05 (s, 10H, Cp), 3.95 (m, 4H, C_5H_4), 3.88 (m, 2 H, C_5H_4). ^{31}P{^{1}H} (81.015 MHz, $CDCl_3$): δ −16.9, −17.5 (4P, AA′BB′, J_{PP} = 28 Hz). Calculated $C_{74}H_{62}IP_4CuFe_2Ru$: C 60.12%; H 4.23%. Found: C 60.38%; H 4.25%.

***trans,trans,trans*-Ru(PBu$_3$)$_2$(CO)$_2$(C≡CFc)$_2$ (3).** A solution of *trans,trans,trans*-$RuCl_2(PBu_3)_2(CO)_2$ (130 mg, 0.21 mmol), FcC≡CSn-(*n*-Bu)$_3$ (250 mg, 0.50 mmol) and CuI (10 mg, 0.05 mmol) was heated to reflux under nitrogen in CH_2Cl_2 (50 mL) for 5.5 h. The red-brown mixture was cooled to 0 °C and filtered through Celite 545. The solution was concentrated to 3−4 mL and CH_3OH was added whereupon the product crystallized as orange needles. The solid was recrystallized from CH_2Cl_2/CH_3OH. Yield: 135 mg (66%). Mp = 140−141 °C. ^{1}H NMR (400 MHz, $CDCl_3$): δ 4.10 (t, J_{HH} = 1.8 Hz, 4 H, C_5H_4), 4.09 (s, 10 H, Cp), 3.96 (t, J_{HH} = 1.8 Hz, 4 H, C_5H_4), 2.05 (m, 12 H, Bu), 1.65 (m, 12 H, Bu), 1.50 (m, 12 H, Bu), 0.99 (t, J_{HH} = 7.3 Hz, 18 H, CH_3, Bu). ^{31}P{^{1}H} NMR (81.015 MHz, $CDCl_3$): δ 13.0 (s, 2 P). Calculated for $C_{50}H_{72}O_2P_2Fe_2Ru$: C 61.31%; H 7.36%. Found: C 60.98%; H 7.33%.

***trans,trans,trans*-Ru(PBu$_3$)$_2$(CO)(py)(C≡CFc)$_2$ (4).** A solution of **3** (50 mg, 0.051 mmol) and pyridine (0.2 mL, 2.5 mmol) was heated at reflux in dry acetone (13 mL) under nitrogen for 15 h. The orange-yellow solution was concentrated to 3−4 mL and CH_3OH was added. The product slowly crystallized at 4 °C to afford orange-red crystals. The solid was recrystallized from CH_2Cl_2/CH_3OH. Crystals of **4** contained 2 equiv H_2O which could not be removed under vacuum. Yield: 40 mg (77%). Mp = 120−122 °C. ^{1}H NMR (400 MHz, $CDCl_3$): δ 10.00 (d, J_{HH} = 5.1 Hz, 2 H, C_5H_5N), 7.70 (t, J_{HH} = 7.5 Hz, 1 H, C_5H_5N), 7.23 (m, 2 H, C_5H_5N), 4.18 (t, J_{HH} = 1.9 Hz, 4H, C_5H_4), 4.15 (s, 10 H, Cp), 4.01 (t, J_{HH} = 1.9 Hz, 4 H, C_5H_4), 1.76 (m, 12 H, Bu), 1.43 (m, 12 H, Bu), 1.28 (m, 12 H, Bu), 0.87 (t, J_{HH} = 7.3 Hz, 18 H, CH_3, Bu). ^{31}P{^{1}H} NMR (81.015 MHz, $CDCl_3$): δ 9.4 (s, 2P). Calculated for $C_{54}H_{81}NO_3P_2Fe_2Ru$: C 60.81%; H 7.60%; N 1.31%. Found: C 61.01%; H 7.45%; N 1.21%.

***trans,trans,trans*-Ru(PBu$_3$)$_2$(CO)(P(OMe)$_3$)(C≡CFc)$_2$ (5).** A solution of **4** (140 mg, 0.134 mmol) and $P(OMe)_3$ (32 μL, 0.27 mmol) was heated at reflux in dry CH_2Cl_2 (15 mL) under nitrogen for 6 h. The orange solution was evaporated to dryness and the oily residue washed with CH_3OH (2 mL) and then dissolved in CH_2Cl_2 (2 mL). CH_3OH (20 mL) was added and the product slowly crystallized at 4 °C as orange-red plates. The solid was recrystallized from CH_2Cl_2/CH_3OH and dried under vacuum for 4 days at 50 °C. Yield: 68 mg (47%). Mp = 101−102 °C. ^{1}H NMR (400 MHz, $CDCl_3$): δ 4.07 (s, 10 H, Cp), 4.03 (t, J_{HH} = 1.7 Hz, 4 H, C_5H_4), 3.92 (t, J_{HH} = 1.7 Hz, 4 H, C_5H_4), 3.68 (d, J_{HP} = 10.2 Hz, 9 H, OMe), 2.04 (m, 12 H, Bu), 1.67 (m, 12 H, Bu), 1.45 (m, 12 H, Bu), 0.96 (t, J_{HH} = 7.3 Hz, 18 H, CH_3,

(26) Manna, J.; John, K. D.; Hopkins, M. D. *Adv. Organomet. Chem.* **1995**, *38*, 79−154.
(27) Osella, D.; Gambino, O.; Nervi, C.; Ravera, M.; Russo, M. V.; Infante, G. *Inorg. Chim. Acta* **1994**, *225*, 35−40.
(28) Colbert, M. C. B.; Lewis, J.; Long, N. J.; Raithby, P. R.; White, A. J. P.; Williams, D. J. *J. Chem. Soc., Dalton Trans.* **1997**, 99−104.
(29) Jones, N. D.; Wolf, M. O.; Giaquinta, D. M. *Organometallics* **1997**, *16*, 1352−1354.
(30) Bartik, T.; Bartik, B.; Brady, M.; Dembinski, R.; Gladysz, J. A. *Angew. Chem., Int. Ed. Engl.* **1996**, *35*, 414−417.
(31) Coat, F.; Lapinte, C. *Organometallics* **1996**, *15*, 477−479.
(32) Brady, M.; Weng, W.; Zhou, Y.; Seyler, J. W.; Amoroso, A. J.; Arif, A. M.; Böhme, M.; Frenking, G.; Gladysz, J. A. *J. Am. Chem. Soc.* **1997**, *119*, 775−788.
(33) Chatt, J.; Shaw, B. L.; Field, A. E. *J. Chem. Soc.* **1964**, 3466−3474.
(34) Smart, J. C.; Pinsky, B. L. *J. Am. Chem. Soc.* **1980**, *102*, 1009−1014.

Bu). $^{31}P\{^1H\}$ NMR (121.5 MHz, $CDCl_3$): δ 7.3 (d, J_{PP} = 48.8 Hz, 2 P, PBu_3), 134.5 (t, J_{PP} = 48.8 Hz, 1 P, $P(OMe)_3$). Calcd for $C_{52}H_{81}O_4P_3Fe_2Ru$: C 58.06%; H 7.54%. Found: C 57.75%; H 7.74%.

{[*cis*-Ru(dppm)$_2$(C≡CFc)$_2$]CuI}(PF$_6$)$_2$ (1^{2+}). A solution of **1** (67 mg, 0.046 mmol) in CH_2Cl_2 (4 mL) was cooled to −78 °C. To this solution was added a solution of ferrocenium hexafluorophosphate (30 mg, 0.091 mmol) in CH_2Cl_2 (3 mL). The solution turned brick-red immediately and was allowed to stir for 2 min at −78 °C. After this period, hexanes (40 mL) were added to precipitate a brick-red solid, which was collected by filtration, washed with hexanes, and dried under vacuum at 80 °C for 3 days. Yield: 71 mg (88%). Calcd $C_{74}H_{62}CuF_{12}Fe_2IP_6Ru$: C 50.26%; H 3.53%. Found: C 50.30%, H 3.53%.

[*trans,trans,trans*-Ru(PBu$_3$)$_2$(CO)$_2$(C≡CFc)$_2$][PF$_6$]$_2$ (3^{2+}). To a solution of **3** (56 mg, 0.057 mmol) in CH_2Cl_2 (2 mL) was added a solution of ferrocenium hexafluorophosphate (38 mg, 0.12 mmol) in CH_2Cl_2 (2 mL). The solution turned red immediately and was allowed to stir for 30 min at room temperature. After this period, hexanes (40 mL) were added to precipitate a brick-red solid, which was collected by filtration, washed with hexanes, and dried under vacuum at 85 °C for 4 days. Yield: 64 mg (88%). Calcd $C_{50}H_{72}F_{12}Fe_2O_2P_4Ru$: C 47.29%; H 5.71%. Found: C 47.15%, H 5.55%.

[*trans,trans,trans*-Ru(PBu$_3$)$_2$(CO)(py)(C≡CFc)$_2$][PF$_6$]$_2$ (4^{2+}). To a solution of **4** (47 mg, 0.046 mmol) in CH_2Cl_2 (2 mL) was added a solution of ferrocenium hexafluorophosphate (30 mg, 0.091 mmol) in CH_2Cl_2 (2 mL). The solution turned purple-red immediately and was allowed to stir for 10 min at room temperature. After this period hexanes (30 mL) were added to precipitate a dark purple solid, which was isolated by filtration and washed with hexanes. The solid was collected by dissolving it in a small amount of CH_2Cl_2, removing the solvent, and drying under vacuum at 90 °C for 7 days. Yield: 48 mg (80%). Calcd $C_{54}H_{77}F_{12}Fe_2OP_4Ru$: C 49.10%; H 5.88%, N 1.06%. Found: C 49.19%; H 6.03%; N 1.04%.

[*trans,trans,trans*-Ru(PBu$_3$)$_2$(CO)(P(OMe)$_3$)(C≡CFc)$_2$][PF$_6$]$_2$ (5^{2+}). Prepared as described for **4**$^{2+}$. Yield: 77%. Calcd $C_{52}H_{81}F_{12}Fe_2O_4P_5Ru$: C 45.73%; H 5.98%. Found: C 45.27%; H 5.85%.

Reaction of 2 with CuI. To a solution of **2** (130 mg, 0.10 mmol) in CH_2Cl_2 (30 mL) was added CuI (38 mg, 0.20 mmol). The suspension was stirred at 25 °C under nitrogen for 24 h. After this period, the solution was filtered through Celite 545. The volume of the filtrate was reduced to approximately 1 mL and hexanes (30 mL) were added to the solution affording a yellow powder, which was washed with hexanes and dried under vacuum at room temperature overnight. Yield: 130 mg (88%).

Reaction of 1 with P(OMe)$_3$. To a solution of **1** (150 mg, 0.10 mmol) in CH_2Cl_2 (25 mL) was added trimethyl phosphite (50 mg, 0.40 mmol). The solution was stirred at 25 °C under nitrogen for 2 days. During this time the reaction became deeper red and cloudy. After this period, the volume of the solution was reduced to approximately 2 mL and diethyl ether (20 mL) was added to the solution yielding an orange powder, which was washed with diethyl ether and dried under vacuum at 85 °C for 2 days. The product was pure **2**. Yield = 82 mg (64%).

Reaction of 4 with CO. Carbon monoxide was gently bubbled throught a stirred solution of **4** (50 mg, 0.051 mmol) in CH_2Cl_2 at room temperature. After 5 h, the product was a mixture of **3** (97%) and **4** (3%) as determined by ^{31}P NMR.

Crystallographic Study. Single crystals of **1**·2($CHCl_3$) were obtained by slow crystallization from layered $CHCl_3$ and hexanes; **3** was crystallized from layered CH_3OH and CH_2Cl_2. Crystal data and refinement parameters are summarized in Table 1. Suitable crystals were mounted on thin, glass fibers with epoxy cement. The systematic absences in the diffraction data and the unit-cell parameters are uniquely consistent with the reported space group. The structures were solved by direct methods, completed by Fourier syntheses, and refined by full-matrix least squares procedures based on F^2. The data were corrected for absorption by using redundant data at different effective azimuthal angles. Two symmetry-unique molecules of cocrystallized chloroform solvent were located in the asymmetric unit of **1**·2($CHCl_3$). The molecule was located at an inversion center for **3**; the unsubstituted cyclopentadienyl ligand was located rotationally disordered in two positions with a 50/50 site occupancy distribution. Cyclopentadienyl groups were refined as idealized, rigid pentagons with librational freedom. All non-hydrogen atoms were refined with anisotropic displacement coefficients. All hydrogen atoms were treated as idealized contributions. All software and sources of atomic scattering factors are contained in the SHELXTL (5.03) program library (G. Sheldrick, Siemens XRD, Madison, WI).

Table 1. Summary of Crystallographic Data for **1**·2($CHCl_3$) and **3**[a]

	1·2($CHCl_3$)	**3**
empirical formula	$C_{76}H_{64}Cl_6CuFe_2IP_4Ru$	$C_{50}H_{72}Fe_2O_2P_2Ru$
formula weight	1717.06	979.79
crystal system	monoclinic	monoclinic
space group	$P2_{1/c}$	$P2_{1/c}$
crystal color	yellow−orange	orange−red
a, Å	17.7522(6)	11.0317(2)
b, Å	17.3529(5)	9.8241(2)
c, Å	23.8798(7)	23.0161(1)
β, deg	90.221(1)	93.117(1)
V, Å^3	7350.7(4)	93.117(1)
D (calcd), g cm^{-3}	1.552	1.306
T_{max}/T_{min}	1.695	1.149
T, K	296	296
radiation	Mo Kα (λ = 0.710 73 Å)	
diffractometer	Siemens CCD	
Z	4	2
μ (Mo Kα), cm^{-1}	16.4	9.74
Θ	1.45−22.50	1.77−28.31
$R(F)$, %	5.24	3.44
$R(wF^2)$, %	12.5	11.7
N_v/N_o	10.5	21.6
goodness-of-fit on F^2	1.08	1.01

[a] Quantity minimized = $R(wF^2) = \sum[w(F_o^2) - F_c^2)^2]/\sum[w(F_o^2)^2]^{1/2}$; $R = \sum\Delta/\sum(F_o)$, $\Delta = |(F_o - F_c)|$. For **1**·2($CHCl_3$): $w = [\sigma^2(F_o^2) + (0.0563P)^2 + 23.7444P]^{-1}$. For **3**: $w = [\sigma^2(F_o^2) + (0.1P)^2]^{-1}$ where P = $(F_o^2 + 2F_c^2)/3$.

Results

Synthesis and Structure of 1. The ruthenium bisacetylide complex **2** was previously synthesized by the CuI catalyzed coupling of FcC≡CSn(*n*-Bu)$_3$ and *cis*-RuCl$_2$(dppm)$_2$.[29] The synthesis of **2** was sensitive to both the amount of CuI used and the reaction temperature. When catalytic CuI (5−25%) was used and the reaction was carried out in 1,2-dichloroethane at reflux, **2** was obtained in good yield. When a stoichiometric amount of CuI was used we observed formation of a mixture of two new complexes with very similar NMR spectra. Elemental analysis of the mixture suggested that the two products were [Ru(dppm)$_2$(C≡CFc)$_2$]CuCl and [Ru(dppm)$_2$-(C≡CFc)$_2$]CuI. By metathesis of the product mixture with NaI we were able to isolate pure [*cis*-Ru(dppm)$_2$(C≡CFc)$_2$]CuI (**1**). Complex **1** was obtained in 70% yield when the reaction was carried out at room temperature in CH_2Cl_2 for 3 days. Complex **1** may also be prepared in 70% yield from FcC≡CSn(*n*-Bu)$_3$ and *trans*-RuCl$_2$(dppm)$_2$ in the presence of excess CuI at room temperature. The X-ray crystal structure of **1**·2($CHCl_3$) shows that the ruthenium center is in a distorted octahedral environment and that the ferrocenylacetylide ligands are in a cis orientation around the ruthenium (Figure 1). The Ru−C bond lengths in **1** are slightly shorter (2.062(8), 2.055(7) Å) than the corresponding bond length in **2** (2.078(7) Å), while the C≡C length is slightly longer in **1** (1.202(10) Å) than in **2** (1.184(8) Å). In addition, both the Ru−C≡C and C≡C−C bond angles are smaller in **1** (168.9(7)° and 160.9(7)°, respectively) compared to the corresponding angles in **2** (174.9(5)° and 173.6(6)°, respectively). The CuI unit is bonded in an η^2 fashion to both acetylide bonds. Many complexes in which Cu is bonded in

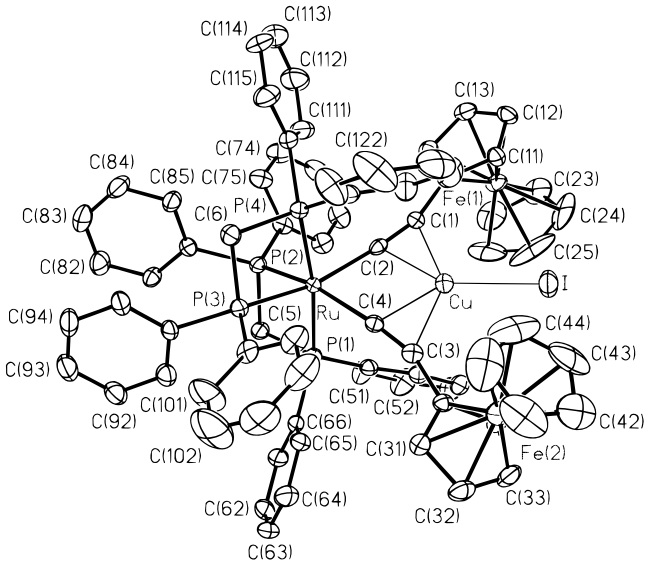

Figure 1. ORTEP diagram of the solid-state structure of **1** (30% probability ellipsoids shown). Hydrogen atoms are omitted for clarity.

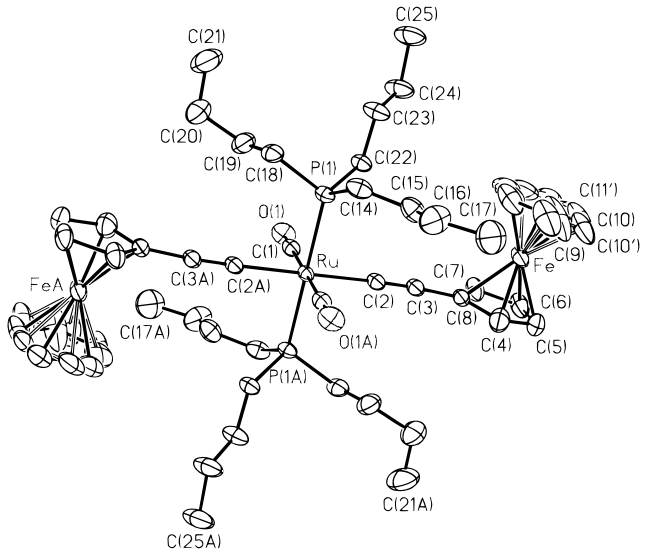

Figure 2. ORTEP diagram of the solid-state structure of **3** (30% probability ellipsoids shown). Both major and minor disordered components of the unsubstituted cyclopentadienyl ligand are depicted. Hydrogen atoms are omitted for clarity.

this manner to an acetylide bond are known,[35−40] however, there are only a few examples of organometallic bidentate bis(alkyne) ligands which chelate Cu^{I}, such as in $[(\eta^5\text{-}C_5H_4SiMe_3)_2Ti(C{\equiv}CSiMe_3)_2]CuOTf$.[41−44]

Isomerization of 1 and 2. To examine the behavior of **1** in the absence of the chelated CuI we attempted to remove the CuI from **1** using $P(OMe)_3$. This method has been used successfully to remove a CuOTf unit from the chelating bis-(η^2-alkyne) unit of $[(\eta^5\text{-}C_5H_4SiMe_3)_2Ti(C{\equiv}CSiMe_3)_2]CuOTf$.[41] The major product of the reaction of **1** with excess $P(OMe)_3$ is **2** (eq 1) (64% isolated yield). When **2** was allowed to react with stoichiometric CuI for 24 h at room temperature we obtained **1** (88% isolated yield).

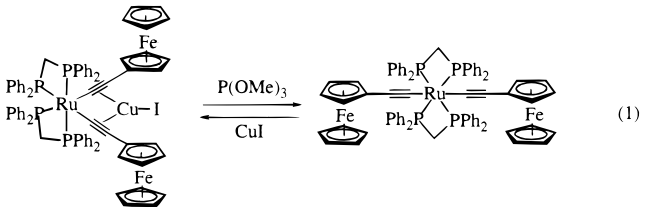

The CuI acts to "lock" the complex in the cis form with the bis(η^2-alkyne) units chelating the CuI. When the CuI is removed from **1** by complexation with $P(OMe)_3$, isomerization to the trans isomer occurs. It is possible that **2** and its cis isomer are in equilibrium, with **2** being the favored form for steric reasons. The chelated CuI must stabilize the cis isomer and trap the cis form as **1**.

Syntheses of 3−5. To examine the effect that the electronic nature of the ancillary ligands on the ruthenium have on the electronic interaction between the ferrocenyl groups we decided to prepare complexes containing phosphines as well as strongly π-acidic ligands such as carbonyls. Initially, we attempted to prepare $Ru(PPh_3)_2(CO)_2(C{\equiv}CFc)_2$; however, we were unsuccessful in preparing this analogue of **2** using the CuI catalyzed coupling route. It was however, possible, to prepare *trans,trans,trans*-$Ru(PBu_3)_2(CO)_2(C{\equiv}CFc)_2$ (**3**) from *trans,trans,trans*-$RuCl_2(CO)_2(PBu_3)_2$ and $FcC{\equiv}CSn(n\text{-}Bu)_3$ using a CuI catalyst. The all trans geometry around the ruthenium was unequivocally established from the X-ray crystal structure of **3** (Figure 2). The structure is similar to that of **2** with the ruthenium in a slightly distorted octahedral environment. The Ru−C bond lengths in **3** are slightly longer (2.095(2) Å) than the corresponding bond length in **2** (2.078(7) Å), while the C≡C length in **3** is 1.200(3) Å.

One of the carbonyl ligands in **3** can be cleanly displaced by reaction with excess pyridine to yield *trans,trans,trans*-$Ru(PBu_3)_2(CO)(py)(C{\equiv}CFc)_2$ (**4**) in 77% yield (eq 2). The structure of **4** may be inferred from the ^{31}P NMR spectrum, which contains only a singlet, and the ^1H NMR spectrum, which shows the ferrocenyl ligands to be equivalent. Assuming the bulky PBu_3 groups are trans as in **3**, the only possible isomer is the all trans form. Complex **3** does not isomerize when heated at reflux in acetone for 24 h. The ligand displacement reaction is reversible and **3** is obtained when CO is bubbled through a solution of **4** at room temperature.

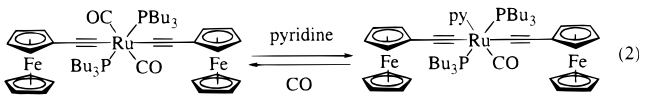

The reaction of **4** with $P(OMe)_3$ in CH_2Cl_2 yields *trans,trans,trans*-$Ru(PBu_3)_2(CO)(P(OMe)_3)(C{\equiv}CFc)_2$ (**5**). Microcrystalline

(35) Yamazaki, S.; Deeming, A. J. *J. Chem. Soc., Dalton Trans.* **1993**, 3053−3057.
(36) Bruce, M. I.; Abu Salah, O. M.; Davies, R. E.; Raghavan, N. V. *J. Organomet. Chem.* **1974**, *64*, C48−C50.
(37) Churchill, M. R.; Bezman, S. A. *Inorg. Chem.* **1974**, *13*, 1418−1427.
(38) Abu Salah, O. M.; Bruce, M. I.; Churchill, M. R.; Bezman, S. A. *J. Chem. Soc., Chem. Commun.* **1972**, 858−859.
(39) Abu Salah, O. M.; Bruce, M. I.; Redhouse, A. D. *J. Chem. Soc., Chem. Commun.* **1974**, 855−856.
(40) Wam, V. W.-W.; Choi, S. W.-K.; Chan, C.-L.; Cheung, K.-K. *Chem. Commun.* **1996**, 2067−2068.
(41) Janssen, M. D.; Herres, M.; Zsolnai, L.; Spek, A. L.; Grove, D. M.; Lang, H.; van Koten, G. *Inorg. Chem.* **1996**, *35*, 2476−2483.
(42) Janssen, M. D.; Köhler, K.; Herres, M.; Dedieu, A.; Smeets, W. J. J.; Spek, A. L.; Grove, D. M.; Lang, H.; van Koten, G. *J. Am. Chem. Soc.* **1996**, *118*, 4817−4829.
(43) Janssen, M. D.; Herres, M.; Spek, A. L.; Grove, D. M.; Lang, H.; van Koten, G. *J. Chem. Soc., Chem. Commun.* **1995**, 925−926.
(44) Janssen, M. D.; Herres, M.; Zsolnai, L.; Grove, D. M.; Spek, A. L.; Lang, H.; van Koten, G. *Organometallics* **1995**, *14*, 1098−1100.

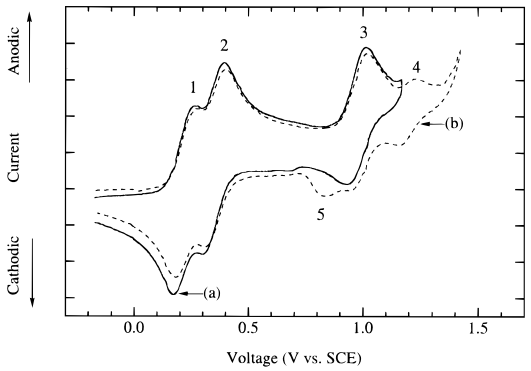

Figure 3. Cyclic voltammogram of **1** in CH_2Cl_2 containing 0.1 M $[(n\text{-}Bu)_4N]PF_6$ from (a) −0.2 to 1.2 V and (b) −0.2 to 1.4 V. Scan rate = 100 mV/s. Wave assignments are discussed in the text.

Table 2. Cyclic Voltammetry Data

complex	$E_{1/2}(1)$,[a] ±0.01 V	$E_{1/2}(2)$,[a] ±0.01 V	$E_{1/2}(3)$ or $E_p(3)$,[a] ±0.01 V	$\Delta E_{1/2}$,[b] ±0.01 V	K_c[c]
1	0.20	0.34	0.97	0.14	260 ± 100
2[d]	0.04	0.26	0.92	0.22	6100 ± 2500
3	0.29	0.38	1.52[e]	0.09	35 ± 15
4	0.22	0.35	1.24[e]	0.13	170 ± 60
5	0.20	0.35	1.30[e]	0.15	370 ± 150
6[f]	0.58	0.68		0.10	52 ± 20

[a] Volts vs SCE, Pt working electrode, CH_2Cl_2 containing 0.1 M $[n\text{-}Bu_4N]PF_6$, 20 °C. [b] $\Delta E_{1/2} = [E_{1/2}(2) - E_{1/2}(1)]$. [c] $\ln(K_c) = nF(\Delta E_{1/2})/RT$. [d] Reference 29. [e] E_p (irreversible wave). [f] Reference 51.

samples of complex **5** were found to have the correct composition by elemental analysis; however, both ^1H and ^{31}P NMR spectra revealed the presence of slight amounts (<5%) of impurities in solution. The impurities are likely structural isomers of **5** since the positions and coupling patterns of the NMR resonances are close to those assigned to **5**. To obtain accurate integrations in the ^{31}P NMR of **5**, the spectrum was acquired by using gated decoupling without NOE with a delay of 5 s.[45]

Cyclic Voltammetry. The cyclic voltammogram (CV) of complex **1** in CH_2Cl_2 containing 0.1 M $[(n\text{-}Bu)_4N]PF_6$ at 20 °C is shown in Figure 3. The CV of **1** contains three quasireversible waves of equal area between 0 and +1.1 V vs SCE (Table 2). The waves at +0.20 V and +0.34 V are assigned to oxidation of the two ferrocenyl centers in bisacetylide **1**. The potentials for the two waves are close to those observed for the two ferrocenyl centers in **2** and are consistent with results observed for related complexes.[46] The difference between the first and second ferrocenyl oxidation waves in **1**, $\Delta E_{1/2}$, is 0.14 V ($\Delta E_{1/2} = E_{1/2}(2) - E_{1/2}(1)$). The redox wave at +0.97 V vs SCE in the CV of **1** is assigned to oxidation of the ruthenium center. This oxidation occurs at a slightly higher potential than the corresponding wave in the CV of complex **2**. When the scan range is extended to +1.4 V vs SCE, a smaller quasireversible wave (wave 4) is observed at +1.18 V, along with a reduction wave (wave 5) at +0.81 V. The relative intensity of wave 4 compared to waves 1−3 in the CV increases with decreasing scan rate, suggesting that wave 4 may be due to oxidation of a product resulting from decomposition of oxidized **1**. Wave 5 may also be due to the decomposition of **1** upon oxidation. This feature was found to grow in intensity upon repeated scanning, possibly the result of deposition of the decomposition product on the working electrode.

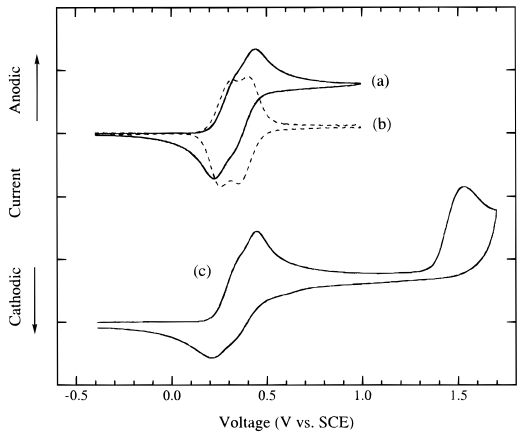

Figure 4. Cyclic voltammogram of **3** in CH_2Cl_2 containing 0.1 M $[(n\text{-}Bu)_4N]PF_6$ from (a) −0.4 to +1.0 V and (c) −0.4 to +1.7 V. Semiderivative of the cyclic voltammogram is shown in (b). Scan rate = 100 mV/s.

The CV of complex **3** also contains three waves (Figure 4c). The closely spaced waves at +0.29 and +0.38 V correspond to oxidation of the two ferrocenyl centers, while the irreversible wave at +1.52 V is assigned to the $Ru^{II/III}$ oxidation. To resolve the closely spaced waves and determine the $E_{1/2}$ values, the semiderivative[47] of the CV was used (Figure 4b). The $Ru^{II/III}$ oxidation potential is higher than that observed for **1** or **2** due to increased back-bonding with the carbonyl ligands in **3**. This wave remained irreversible at faster scan rates (up to 1000 mV/s) or low temperature (−78 °C). The CVs of **4** and **5** are similar to that of **3** and contain two closely spaced ferrocenyl oxidations and an irreversible ruthenium oxidation wave at higher potential. The oxidation potentials for **4** and **5** are shown in Table 2. Only the complexes which contain carbonyl ligands have an irreversible oxidation wave for the ruthenium center. It is likely that in these complexes the electron is removed from an orbital on the Ru which is involved in metal−carbonyl bonding, thus weakening the bond and causing decomposition.

Spectroscopic Characterization. Chemical oxidation of one or both ferrocenyl groups in the complexes described herein allows the spectroscopic properties of the oxidized species to be measured and compared with those of the neutral analogues. Shifts in diagnostic absorptions in the IR region as well as the appearance of intervalence charge-transfer bands in the near-IR are useful in evaluating the extent of electronic delocalization in these complexes.

The dications of **1**−**5** were prepared by oxidation with 2 equiv of $FcPF_6$ and were isolated as stable solids, which were characterized by elemental analysis. The dications were shown to be paramagnetic at room temperature using the Evans NMR method,[48] and thus NMR spectroscopy was not useful in characterizing the oxidized species. The monocations of **1**−**5**, prepared by dissolving equimolar masses of the neutral complex and the corresponding dication in the appropriate solvent, are in equilibrium with the corresponding neutral and dicationic species (eq 3). The equilibrium constants (K_c) for **1**−**5** at 20 °C may be calculated from $\Delta E_{1/2}$ by using the Nernst equation[49] and are shown in Table 2.

(45) Verkade, J. G.; Quin, L. D. *Phosphorus-31 NMR Spectroscopy in Stereochemical Analysis*; VCH: Deerfield Beach, FL, 1987.
(46) Colbert, M. C. B.; Ingham, S. L.; Lewis, J.; Long, N. J.; Raithby, P. R. *J. Chem. Soc., Dalton Trans.* **1994**, 2215−2216.
(47) Rieger, P. H. *Electrochemistry*; Chapman & Hall: New York, 1994.
(48) Evans, D. F. *J. Chem. Soc.* **1959**, 2003−2005.
(49) $\ln(K_c) = nF(\Delta E_{1/2})/RT$.

$$X^{2+} + X \overset{K_c}{\rightleftharpoons} 2X^{+} \quad (3)$$

The visible and IR spectroscopic data for the neutral and oxidized species are collected in Table 3. The visible spectra of the neutral complexes **1**−**5** all contain ligand-based absorptions (data not shown) in addition to weaker bands (430−460 nm) assigned to metal d−d transitions. The monocations (**1**$^+$−**5**$^+$) of these species all exhibit medium intensity transitions in the visible region between 500 and 620 nm, which are assigned to a ferrocenium-based ligand-to-metal charge transfer (LMCT) excitation. This assignment is based on the similarity of the energy and intensity of the band to that observed for ferrocenium (620 nm).[50] The energy of the LMCT absorption of ferrocenium blue-shifts with the introduction of electron-withdrawing substituents[50] and is observed at 510 nm in [Fc−C≡C−C≡C−Fc]$^+$ (**6**$^+$).[51]

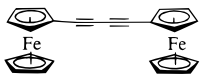

6

The LMCT absorptions for the monocations **1**$^+$−**5**$^+$ appear at higher wavelengths than the absorption for **6**$^+$, consistent with electron donation from the ruthenium moiety to the ferrocenium. In the visible spectra of the dications **1**$^{2+}$−**5**$^{2+}$ the LMCT absorption is blue-shifted with respect to the corresponding monocation, consistent with competition by the two ferrocenium groups for the electron density of the ruthenium center. Significantly, the absorption maximum for the LMCT transition is sensitive to the electronic nature of the ancillary ligands found around the ruthenium center. Within the series of monocations of the trans substituted complexes, λ_{max} for the LMCT absorption decreases in the order: **2**$^+$ > **4**$^+$ ≈ **5**$^+$ > **3**$^+$. The same trend is observed within the series of dications.

In the infrared region the strong absorptions due to the C≡C and C≡O groups are useful, since their positions are sensitive to the electron density at the ruthenium center. The energy of the acetylide absorption ($\nu_{C\equiv C}$) increases in the series of trans bisacetylide complexes as the number of electron-withdrawing carbonyl ligands on the metal increases ($\nu_{C\equiv C}$: **2** < **4** ≈ **5** < **3**). The energy of the absorption due to the carbonyl group ($\nu_{C\equiv O}$) is sensitive to the degree of back-bonding to the ligand trans to the carbonyl. Thus $\nu_{C\equiv O}$ in **4**, which has a σ-donor (pyridyl) trans to the carbonyl, is lower than $\nu_{C\equiv O}$ in **5** in which the trans P(OMe)$_3$ is a weak π-acceptor. The carbonyl absorption in **3** has the highest wavenumber of the series, as the two trans carbonyls compete for back-bonding from the same Ru d-orbital. The acetylide absorption in the spectra of the dications (**1**$^{2+}$−**5**$^{2+}$) is shifted to lower energy than the absorption for the analogous neutral complexes as more electron density from the ruthenium is transferred to the acetylide bond via increased back-bonding. This is also observed in the carbonyl stretching frequency in **3**$^{2+}$−**5**$^{2+}$ which increases slightly relative to the neutral analogues as less electron density is available for back-bonding with the carbonyl groups upon oxidation of the ferrocenyl groups.

Most mixed-valence complexes exhibit absorptions in the visible or near-IR region corresponding to intervalence charge-transfer (IVCT) absorptions.[6,52,53] The energies and intensities of these absorptions have been used to classify mixed-valence complexes according to the degree of delocalization they exhibit. Completely localized (class I) mixed-valence complexes rarely have IVCT transitions, while completely delocalized (class III) complexes may have visible or near-IR absorptions. Many complexes are partially delocalized (class II) and frequently display IVCT absorptions in the visible or near-IR regions. Several diagnostic tests are available for classification of mixed-valence complexes according to the theory developed by Hush.[6,52,53]

Table 3. Visible and Infrared Data

complex	visible λ_{max}, nm (±5 nm); (ϵ (M^{-1} cm^{-1}) ±5%)[a]	IR, cm^{-1} (±5 cm^{-1})[b]
1	460 (850)	1994
1$^+$	500 (4700)	
1^{2+}	378 (7700), 476 (sh) (8500)	1948
2	434 (2000)	2067
2$^+$	448 (sh) (2100), 616 (4100), 820 (sh) (1800)	
2^{2+}	420 (sh) (5500), 560 (13 000)	1997
3	450 (760)	2103 (C≡C), 1986 (C≡O)
3$^+$	390 (sh) (5100), 514 (6900)	
3^{2+}	378 (10 000), 488 (12 000)	2067 (C≡C), 1994 (C≡O)
4	450 (920)	2079 (C≡C), 1940 (C≡O)
4$^+$	420 (sh) (3400), 570 (5300)	
4^{2+}	394 (sh) (8500), 524 (12 000)	2030 (C≡C), 1954 (C≡O)
5	454 (810)	2084 (C≡C), 1974 (C≡O)
5$^+$	414 (sh) (3700), 562 (5300)	
5^{2+}	394 (sh) (7500), 524 (9100)	2032 (C≡C), 1979 (C≡O)

[a] Solvent: CH_2Cl_2. [b] KBr.

Table 4. Near-IR Data for Monocations

complex	ν_{max}, cm^{-1} (±50 cm^{-1}) (λ_{max}, nm)[a]	ϵ_{max}, M^{-1} cm^{-1} (±5%)	$\Delta\nu_{1/2}$, cm^{-1} (±50 cm^{-1})	$\alpha^2 \times 10^{-3}$ (±10%)[b]
1$^+$	8420 (1190)	440	2400	1.4
	5630 (1775)	290	2100	1.2
	4320 (2315)	310	810	
2$^+$	4770 (2095)	6700	3300	47
	4380 (2285)	2700	700	
3$^+$	8030 (1245)	2400	3500	12
	4380 (2285)	410	540	
4$^+$	6430 (1555)	3200	2900	16
	4410 (2265)	1100	510	
5$^+$	6520 (1535)	2900	3100	15
	4440 (2250)	1100	530	

[a] CH_2Cl_2, 20 °C. [b] $\alpha^2 = [(4.2 \times 10^{-4})\epsilon_{max}\Delta\nu_{1/2}]/\nu_{max}d^2$.

The near-IR data for the monocations and dications are shown in Tables 4 and 5, respectively. None of the neutral complexes absorb in the near-IR region. The spectra of the monocations and dications all contain multiple absorption bands in the near-IR region. For these absorptions, the bandwidths at half-maximum ($\Delta\nu_{1/2}$) were measured directly when possible and by using Gaussian peak fitting when necessary in the cases of overlapping bands. The spectra were obtained in a range of solvents in order to study the solvent dependence of the observed transitions. The lower energy band was obscured by solvent overtones in many solvents, therefore data for this band are shown only for spectra taken in CH_2Cl_2. The spectra of **1**$^+$ and **1**$^{2+}$ were only obtained in CH_2Cl_2 and 1,2-dichloroethane because the complexes decomposed or reacted with most other solvents.

The near-IR spectra of all the mono- and dications contain a higher energy band (4770−9620 cm^{-1}) and a lower energy band (4260−4470 cm^{-1}). The spectrum of **1**$^{1+}$ has a third broad absorption. Representative spectra for complexes **4**$^+$ and **4**$^{2+}$

(50) Geoffroy, G. L.; Wrighton, M. S. *Organometallic Photochemistry*; Academic Press: New York, 1979.
(51) Levanda, C.; Bechgaard, K.; Cowan, D. O. *J. Org. Chem.* **1976**, *41*, 2700−2704.
(52) Creutz, C. *Prog. Inorg. Chem.* **1983**, *30*, 1−73.
(53) Crutchley, R. J. *Adv. Inorg. Chem.* **1994**, *41*, 273−325.

Table 5. Near-IR Data for Dications

complex	solvent[a]	ν_{max}, cm^{-1} ($\pm$50 cm^{-1}) (λ_{max}, nm)	ϵ_{max}, M^{-1} cm^{-1} ($\pm$5%)	$\Delta\nu_{1/2}$, cm^{-1} ($\pm$50 cm^{-1})	$\alpha^2 \times 10^{-3}$ ($\pm$10%)[b]
$\mathbf{1}^{2+}$	CH_2Cl_2	9620 (1040)	1600	3200	5.8
		4260 (2350)	150	950	
	$ClCH_2CH_2Cl$	9260 (1080)	1800	3600	7.5
$\mathbf{2}^{2+}$	CH_2Cl_2	6650 (1505)	7400	2800	33
		4470 (2240)	2400	480	
	CH_3COCH_3	6850 (1460)	7500	2800	32
	$ClCH_2CH_2Cl$	6540 (1530)	6400	2800	29
	1,2-dichlorobenzene	6210 (1610)	5500	3800	36
	chlorobenzene	6120 (1635)	5600	4400	42
	CH_3CN	6950 (1440)	7800	2600	31
	nitrobenzene	6780 (1475)	10000	2100	34
	1,1,2-trichloroethylene	6170 (1621)	6300	3500	37
	CH_3NO_2	6900 (1450)	8400	2600	33
$\mathbf{3}^{2+}$	CH_2Cl_2	9220 (1085)	3700	2800	12
		4290 (2330)	340	840	
$\mathbf{4}^{2+}$	CH_2Cl_2	7940 (1260)	5200	2900	21
		4360 (2295)	860	570	
$\mathbf{5}^{2+}$	CH_2Cl_2	7880 (1270)	3500	3200	16
		4370 (2290)	620	640	

[a] 20 °C. [b] $\alpha^2 = [(4.2 \times 10^{-4})\epsilon_{max}\Delta\nu_{1/2}]/\nu_{max}d^2$.

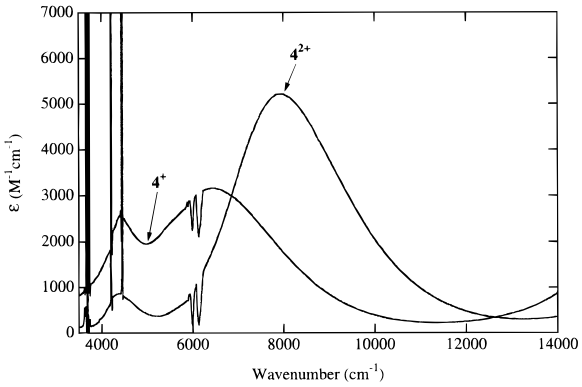

Figure 5. Near-IR spectra of $\mathbf{4}^{+}$ and $\mathbf{4}^{2+}$ in CH_2Cl_2. Sharp absorptions are due to vibrational overtones from the solvent.

are shown in Figure 5. The higher energy band is assigned to a class II IVCT transition. The half-widths (2100−4400 cm^{-1}) and intensities of the high energy band are consistent with this assignment. In addition, the absorption maximum of the band depends both on solvent and on the ancillary ligands around the ruthenium (*vide infra*), also consistent with the band being due to an IVCT transition. The lower energy band is narrower (480−950 cm^{-1}) and of lower intensity than the high energy band, while the absorption maximum for the lower energy band is relatively insensitive to changes in substituents on the ruthenium center. Because of vibrational overtones from the solvent the absorption maximum of the low energy band could only be observed in a limited number of solvents; however, from these data it is clear that the absorption band is largely solvent independent.

Although it is difficult to unequivocally assign the lower energy band, it is clear that the properties of the low energy absorption differ dramatically from the behavior of the high energy band. It is most likely that the low energy band is due to a d−d transition in Fe^{III} which becomes accessible in the mono- and dicationic species. The energy of such a band would be expected to be solvent independent[54] and to appear at approximately the same energy for all the mono- and dications. In addition, since the electronic transition is localized on the Fe^{III} it would be relatively independent of changes in the

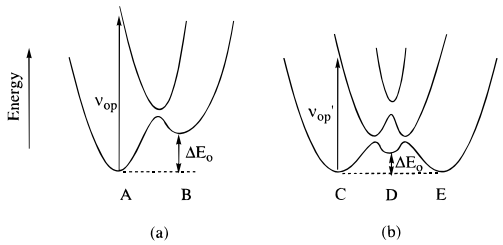

Figure 6. Potential energy diagrams for initial and final states for (a) states A and B and (b) states C, D, and E.

ancillary ligands on the Ru center. Multiple bands in other mixed valent complexes have been assigned to either ligand-field splitting[55] or spin−orbit coupling[56] in the metal centers. The markedly different behavior of the two absorption bands in the series of complexes described herein makes these explanations less likely. The low energy absorption is not due to intermolecular charge transfer as the relative band intensities do not exhibit a concentration dependence, and the spectra are taken at low concentrations (10^{-4} − 10^{-3} M).

The higher energy near-IR absorption band for the dications $\mathbf{2}^{2+}$−$\mathbf{5}^{2+}$ (4770−9620 cm^{-1}) are assigned to the IVCT transition shown in eq 4. In these complexes both iron centers are present as Fe^{III} and thus IVCT between iron centers is not possible.

$$\underset{A}{Fe^{III}—Ru^{II}—Fe^{III}} \xrightarrow{\nu_{op}} \underset{B^*}{[Fe^{III}—Ru^{III}—Fe^{II}]^*} \qquad (4)$$

The absorption maximum (ν_{max}) for the IVCT band shifts to higher energy as the number of carbonyl ligands on the ruthenium increases (ν_{max}: $\mathbf{2}^{2+} < \mathbf{4}^{2+} \approx \mathbf{5}^{2+} < \mathbf{3}^{2+}$). The origin of this shift in ν_{max} may be considered by using two overlapping potential energy curves (Figure 6a). In this diagram ν_{op} is the energy required to excite an electron from state A to state B. For complexes $\mathbf{2}^{2+}$−$\mathbf{5}^{2+}$ ν_{op} should vary proportionally with the difference in ground-state energies (ΔE_o). Importantly, ΔE_o is expected to be larger as the electron density at the ruthenium is decreased via electron accepting ligands.

It is not possible to calculate ΔE_o exactly from the measured oxidation potentials since state B cannot be isolated; however,

(54) Lever, A. B. P. *Inorganic Electronic Spectroscopy;* 2nd ed.; Elsevier: New York, 1984.

(55) Creutz, C. *Inorg. Chem.* **1978**, *17*, 3723−3725.

(56) Kober, E. M.; Goldsby, K. A.; Narayana, D. N. S.; Meyer, T. J. *J. Am. Chem. Soc.* **1983**, *105*, 4303−4309.

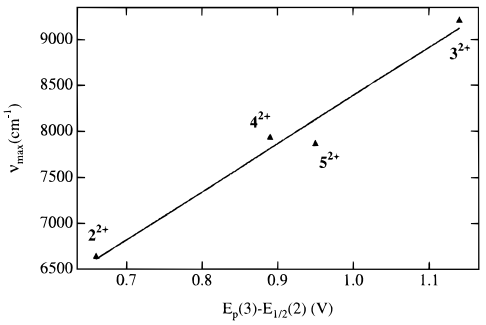

Figure 7. Plot of $E_p(3) - E_{1/2}(2)$ vs ν_{max} (near-IR) for the dications $\mathbf{2}^{2+}-\mathbf{5}^{2+}$ in CH_2Cl_2.

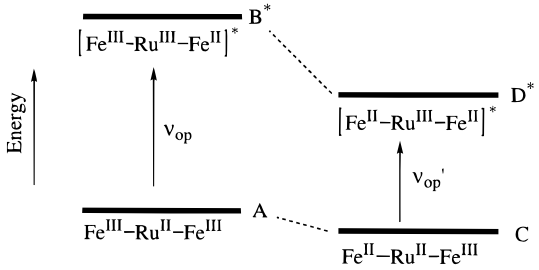

Figure 8. Relative energy diagram for states A−D.

we may estimate ΔE_o from the electrochemical data. The transition from state A to B involves oxidation of the Ru^{II} and concomitant reduction of the Fe^{III} center. ΔE_o will therefore be proportional to the difference between the $Ru^{II/III}$ and the second $Fe^{II/III}$ oxidation potential (eq 5).

$$\Delta E_o \propto E_p(3) - E_{1/2}(2) \tag{5}$$

Since ν_{op} is proportional to ΔE_o a plot of ν_{max} for the dications vs $E_p(3) - E_{1/2}(2)$ should be linear. These data are plotted in Figure 7 and demonstrate an approximately linear correlation between ν_{max} and $E_p(3) - E_{1/2}(2)$.

The model shown in Figure 6a may be extended to charge transfer in the monocations (eq 6).

$$\underset{C}{Fe^{II}-Ru^{II}-Fe^{III}} \xrightarrow{\nu_{op}'} \underset{D^*}{[Fe^{II}-Ru^{III}-Fe^{II}]^*} \rightarrow \underset{E}{Fe^{III}-Ru^{II}-Fe^{II}} \tag{6}$$

Here one must consider a three-state potential energy diagram (Figure 6b) in which ν_{op}' corresponds to the energy required to optically excite an electron from state C to D. State C and E are isoenergetic, while state D has a higher ground-state energy. The absorption maximum for the IVCT band is lower by 1000−2000 cm^{-1} than the corresponding transition in the spectra of the corresponding dications. The relative magnitude of the absorption maxima in the spectra of the mono- and dications may be predicted by considering the relative energies of the states involved (Figure 8). Both states C and D are lower in energy than states A and B, respectively, because C and D carry less total charge than A and B. Furthermore, oxidation of an Fe^{II} adjacent to a Ru^{III} (D to B) requires more energy than oxidition of an Fe^{II} adjacent to a Ru^{II} (C to A). Thus ν_{op}' is expected to be lower in energy than ν_{op}. A transition involving long-range electron transfer between the two iron centers is also possible but is expected to be of significantly higher energy because the distance between Fe centers in these molecules is large. For comparison the IVCT band in the spectrum of $\mathbf{6}^+$, in which the Fe−Fe distance is significantly shorter than in $\mathbf{2}^+-\mathbf{5}^+$, is observed at 1180 cm^{-1}.[51] A near-IR absorption was also

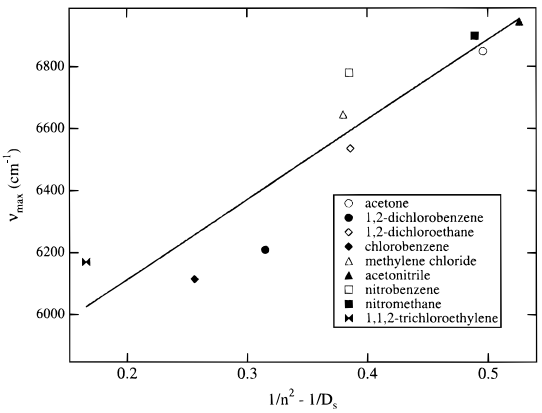

Figure 9. Plot of $1/n^2 - 1/D_s$ vs ν_{max} (near-IR) for $\mathbf{2}^{2+}$.

observed in mixed valent diferrocenylpolyenes,[57] however, the intermetallic distance in solution in these complexes is not known exactly due to the nonrigidity of the polyene linker. In the visible spectrum only $\mathbf{2}^+$ exhibits an unusual band at 820 nm, it is possible that this band arises from direct iron to iron charge transfer. Since states C and E are isoenergetic, state D can relax thermally to either C or E. Optical excitation to form state D followed by electron transfer to form E thus provides a pathway for charge transfer across the ruthenium bisacetylide bridge.

The dependence of the ν_{max} of an IVCT band on solvent has been used as a diagnostic test of a class II species.[6,52,53] According to the Hush model, the energy of an IVCT transition for a weakly coupled asymmetric system, E_{op}, is related to the inner and outer reorganizational parameters, λ_i and λ_o, by eq 7. Additional energy terms are added to take into account the difference in ground-state energies (ΔE_o) and excitation to either a spin−orbit or ligand-field excited state ($\Delta E'$).

$$E_{op} = \lambda_i + \lambda_o + \Delta E' + \Delta E_o \tag{7}$$

$$\lambda_o = (me)^2(1/r - 1/d)(1/n^2 - 1/D_s) \tag{8}$$

The dielectric continuum treatment defines the outer-sphere reorganization energy according to eq 8, in which m is the number of electrons transferred, e is the electron charge, r is the difference in molecular radii of the redox sites, d is the internuclear separation, n is the refractive index, and D_s is the static dielectric constant of the solvent. If λ_o is assumed to be the only solvent dependent term in eq 7, then ν_{max} may be expected to vary linearly with $(1/n^2 - 1/D_s)$ for a class II system. The spectra of the dications $\mathbf{2}^{2+}-\mathbf{5}^{2+}$ all exhibit shifts in ν_{max} as a function of solvent. A plot of ν_{max} as a function of $(1/n^2 - 1/D_s)$ for $\mathbf{2}^{2+}$ is shown in Figure 9, along with the best-fit line obtained from linear regression. This plot is consistent with complex $\mathbf{2}^{2+}$ behaving as a class II partially delocalized system.

The energy and intensities of the near-IR absorptions of mixed-valence complexes may be used to calculate an interaction parameter α^2, which is a measure of the delocalization in the ground state (eq 9).[6]

$$\alpha^2 = [(4.2 \times 10^{-4})\epsilon_{max}\Delta\nu_{1/2}]/\nu_{max}d^2 \tag{9}$$

In this equation $\Delta\nu_{1/2}$ is the half-width of the IVCT absorption band, d is the distance between donor and acceptor wave functions in angstroms which we estimate as the intermetallic distance. The values calculated for α^2 are shown in Tables 4

(57) Ribou, A. C.; Launay, J. P.; Sachtleben, M. L.; Li, H.; Spangler, C. W. *Inorg. Chem.* **1996**, *35*, 3735−3740.

and 5. The value used for the Ru−Fe intermetallic distance was obtained from the structural data for **1**−**3**; complexes **4** and **5** were assumed to have the same intermetallic distance as **3**. The calculated values of α^2 for the monocations $\mathbf{3}^+$−$\mathbf{5}^+$ are similar, while the value obtained for $\mathbf{2}^+$ is higher. The monocation $\mathbf{1}^+$ has two broad IVCT absorptions which have similar α^2 values, both being lower than those calculated for $\mathbf{2}^+$−$\mathbf{5}^+$. In the series of dications, α^2 was also largest for $\mathbf{2}^{2+}$ and smallest for $\mathbf{1}^{2+}$. The differences between the interaction parameters for the monocations and dications are inconclusively small due to the error arising from the estimate of d as the intermetallic distance. The error involved in calculating α^2 makes this parameter less useful in comparing a series of molecules with closely related structures; however, comparisons with other molecules containing the same metal centers are instructive. The α^2 value for $[(\eta\text{-}C_5H_5)(PPh_3)_2RuC{\equiv}CFc]^+$ is 2.8×10^{-2},[58] comparable to the values for $\mathbf{2}^+$−$\mathbf{5}^+$, while α^2 for $[(NH_3)_5RuNCFc]^+$ is only 2.3×10^{-3}.[59] The smaller values of α^2 for $\mathbf{1}^+$ and $\mathbf{1}^{2+}$ were obtained even though the extent of delocalization observed from cyclic voltammetry of **1** is comparable to that for **4** and **5**. Complex **1** contains a coordinated Cu which can interact with the delocalized system and decrease the effective distance between the donor and acceptor wave functions.

Discussion

The cyclic voltammetric and spectroscopic data for **1**−**5** and their oxidized derivatives may be used to compare the electronic delocalization within this series of complexes. Complex **1** demonstrates the effect of varying the geometry at the ruthenium on the electronic delocalization. For **1**, $\Delta E_{1/2}$ is 0.14 V, significantly smaller than $\Delta E_{1/2}$ observed for **2** (0.22 V). There are two factors which may influence $\Delta E_{1/2}$ here: the geometry around the ruthenium center and the presence of the chelated CuI. In complex **2** the electronic interaction between the terminal redox groups occurs via the π bonds of the cyclopentadienyl and alkynyl moieties and the d-orbitals of the ruthenium. When the acetylide ligands are trans, as in **2**, the same d-orbitals on the metal are involved in back-bonding to both acetylide ligands ($d_{xz} \rightarrow \pi^*$ and $d_{xy} \rightarrow \pi^*$). This should enhance the interaction between the ferrocenyl groups in **2** relative to **1**, where the acetylide ligands are cis, and back-bonding involves three different d-orbitals, only one of which is common to both acetylide ligands ($d_{xy} \rightarrow \pi^*$, $d_{xz} \rightarrow \pi^*$ for one acetylide, $d_{xy} \rightarrow \pi^*$, $d_{yz} \rightarrow \pi^*$ for the other).

The chelated CuI in **1** could act either to enhance electronic interaction between the ferrocenyl groups by acting as a second bridge between the two C≡C bonds, or to reduce the interaction through the ruthenium center by reducing conjugation between the ferrocenyl group and the ruthenium. It is difficult to predict which effect is more significant without comparing the electrochemical behavior of the analogue of **1** in which the CuI has been removed; however, this was not possible due to the instability of that complex. In the analogous complex $[(\eta^5\text{-}C_5H_4SiMe_3)_2Ti(C{\equiv}CSiMe_3)_2]CuOTf$[41−44] the coordinated CuOTf group lowers the energy of the C≡C absorption in the IR relative to the free ligand. This was interpreted as a result of both back-bonding from the Cu^I to a π^* orbital on the ligand, as well as donation from the π bond to the Cu^I. These results suggest that electronic interaction via the coordinated Cu^I in **1** is possible, but the magnitude of this effect relative to interaction through the Ru center is difficult to predict.

The behavior of the series of trans bisacetylide complexes **2**−**5** may be directly compared as the basic structure of these complexes is identical. From cyclic voltammetry, we observe that $\Delta E_{1/2}$ decreases as **2** > **5** ≈ **4** > **3**. Considering the properties of the ancillary ligands on the ruthenium found in this series of complexes, pyridine is a σ-donor and the phosphines are strong σ-donors and weak π-acceptors, while carbonyl is a strong π-acceptor and a weak σ-donor. Our results demonstrate that the electronic interaction between the ferrocenyl groups depends primarily on the number of carbonyl ligands. Hence, the more carbonyl ligands present around the ruthenium, the smaller $\Delta E_{1/2}$. We view this as resulting primarily from the strongly π-acidic nature of the carbonyl groups, which serve to withdraw electron density from the ruthenium and thus decrease the electron density available for conjugation with the acetylide bonds. Varying the number and nature of the non-carbonyl ligands has only a small effect on delocalization compared to the effect exerted by the carbonyl groups. For example, the PBu_3 groups are slightly better σ-donor ligands than the dppm groups, yet the increased electron density contributed by the PBu_3 ligands is negligible compared to that removed by the carbonyl ligand(s). In addition to the trend in $\Delta E_{1/2}$ the potential measured for the $Ru^{II/III}$ oxidation wave in the CV increases as the number of carbonyl ligands on the ruthenium is increased. As electron density is lost from the metal to the carbonyl ligands, the ruthenium becomes increasingly difficult to oxidize.

The trends in electron delocalization observed by cyclic voltammetry are consistent with those observed by spectroscopic methods. In the visible region, the magnitude of the red-shift observed in the LMCT band for $\mathbf{2}^+$−$\mathbf{5}^+$ relative to $\mathbf{6}^+$ increases as the number of donor ligands on the ruthenium is increased. Similarly, in the infrared region both the C≡C and C≡O absorptions correlate to the electrochemical results. Based on the CV data, **2** has increased electron density at the ruthenium relative to the monocarbonyl complexes **4** and **5** and dicarbonyl **3**. This results in a lower $\nu_{C\equiv C}$ for **2** than for **4** or **5** since more ruthenium acetylide back-bonding is possible in **2**. Complex **4** also has a donor ligand trans to the carbonyl which allows more back-bonding to the lone carbonyl group than in **3**. Interestingly, the wavenumber difference between the acetylide absorption of the dicationic and neutral species correlates with the degree of electronic delocalization observed in the CV. Thus **2** has the largest $\Delta E_{1/2}$ and the difference in the C≡C absorption is 70 cm^{-1} between **2** and $\mathbf{2}^{2+}$, while **3** has the smallest $\Delta E_{1/2}$ and the difference between the IR absorptions of **3** and $\mathbf{3}^{2+}$ is 36 cm^{-1}. This is a result of how much of the electron density at ruthenium is available for back-bonding with the acetylide ligands. Ancillary ligands such as carbonyl which withdraw electron density make the ruthenium d-electrons less likely to participate in electron transfer along the acetylide backbone.

The electron delocalization in these complexes is best explained by the potential energy diagram shown in Figure 6b. The nature of the ancillary ligands on the ruthenium center affects the difference in ground-state energy (ΔE_o). Donor ligands decrease ΔE_o, thus facilitating electron transfer across the ruthenium bisacetylide bridge, while acceptor ligands increase ΔE_o. Complex **6**, in which the ferrocenyl groups are bridged by a 1,3-butadiynyl moiety, shows less electron delocalization (as estimated by $\Delta E_{1/2}$) than **2**, **4**, or **5** and is comparable to **3**. This result may be explained by considering the potential energy diagram for $\mathbf{6}^+$ (Figure 10a). Electron transfer between the two states occurs either in the ground state by overcoming the activation barrier (E_{th}) or in the excited state

(58) Sato, M.; Shintate, H.; Kawata, Y.; Sekino, M.; Katada, M.; Kawata, S. *Organometallics* **1994**, *13*, 1956−1962.

(59) Dowling, N.; Henry, P. M.; Lewis, N. A.; Taube, H. *Inorg. Chem.* **1981**, *20*, 2345−2348.

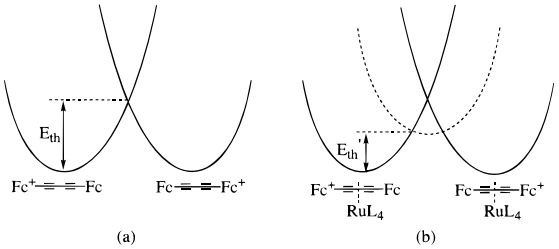

Figure 10. Potential energy diagram for electron delocalization in (a) $\mathbf{6}^+$ and in a hypothetical molecule in which a RuL_4 is inserted into the central C−C bond in $\mathbf{6}^+$.

via IVCT. Figure 10b shows the potential energy diagram for a hypothetical molecule consisting of $\mathbf{6}^+$ with a ruthenium center between the two ferrocenyl groups. Here the ruthenium facilitates electron delocalization by reducing the energy barrier in the ground state (E_{th}'). The potential energy diagrams for the mono- and dications of complexes **2**−**5** (Figure 6a,b) are slightly different since the distance between iron centers is greater than that shown in Figure 10b; however, the same principle is expected to hold. Our results clearly demonstrate that the extent to which the energy barrier is lowered is influenced by the ancillary ligands on the ruthenium, and therefore the extent of delocalization is affected by these ligands.

Acknowledgment. We are grateful to the UBC Chemistry Department and the Natural Sciences and Engineering Research Council of Canada for funding.

Supporting Information Available: A listing of tables of crystal data, positional parameters, bond distances and angles, and anisotropic thermal parameters for **1** and **3** and a complete table of near-IR spectral data (23 pages). See any current masthead page for ordering and Internet access instructions.

JA9732486